Manipulation of Non-Magnetic Microbeads using Soft Microrobotic Sperm

Ahmad E. El-Etriby*, Anke Klingner*, Ahmet Fatih Tabak†, and Islam S. M. Khalil*

***Abstract*— In this work, we demonstrate the ability of soft microrobotic sperms to manipulate non-magnetic microbeads in two-dimensional space. First, we model the interaction between the microrobotic sperm and microbeads using the resistive-force theory (RFT). This RFT-based model enables us to predict the maximum payload a soft microrobotic sperm can manipulate at different actuation frequencies. Second, we demonstrate manipulation of the microbeads using microrobotic sperm under the influence of controlled magnetic fields. Our teleoperation manipulation trials show that the microrobotic sperm swims at an average speeds of 0.16 and 0.035 body-length-per-second during collision-free locomotion and manipulation, respectively. In addition, the microrobotic sperm positions 2-microbead within the vicinity of a reference position with maximum steady-state error of 55 μm.**

I. Introduction

Recently, considerable progress has been accomplished in the fabrication and control of biologically inspired microrobots to achieve non-trivial tasks at low-Reynolds numbers. The swimming methods of biologically inspired microrobots capitalize mainly on either helical propulsion or travelling wave propulsion [1]. The former method uses screw-shaped swimmers driven using rotating magnetic fields, while the later method depends on elastic-tail swimmers driven by periodic magnetic fields. Several microswimmer designs have been presented based on helical and travelling wave propulsion. One method to construct a helical microswimmer combines a magnetic head to a helical body such that its magnetization is perpendicular to the long axis of the helix [2]-[5]. Similarly to this method, elastic-tail swimmers can also be constructed by the deposition of a magnetic layer on the proximal end of an elastic filament [6]-[11]. These realization studies have been followed by other novel actuation methods (based on acoustic waves [12] and light [13]) and a series of attempts to translate these swimmers into biomedical [5], [14] and nano-technology applications [15].

Here, we study the influence of a payload (non-magnetic microbeads) on the flagellar propulsion of a soft microrobotic sperm driven using periodic magnetic fields. We model the microrobotic sperm and the payload using the resistive-force theory (RFT) to predict the influence of a payload on the flagellar propulsion [16]. We also demonstrate manipulation of microbeads in two-dimensional space (see Fig. 1), and compare our experimental results to the theoretical prediction of our RFT-based model. The remainder of the paper is organized as follows: Section II provides a theoretical picture for the propulsion of the microrobotic sperm with a payload. Experimental results are included in Section III. Finally, Section IV concludes and provides directions for future work.

This work was supported by the DAAD-BMBF funding project and the Science and Technology Development Fund in Egypt (No. 23016).

*The authors are affiliated with the German University in Cairo, 11835 Cairo, Egypt.

†The author is affiliated with the Mechatronics Engineering Department, Faculty of Engineering, Okan University, 34959 Tuzla, Istanbul, Turkey.

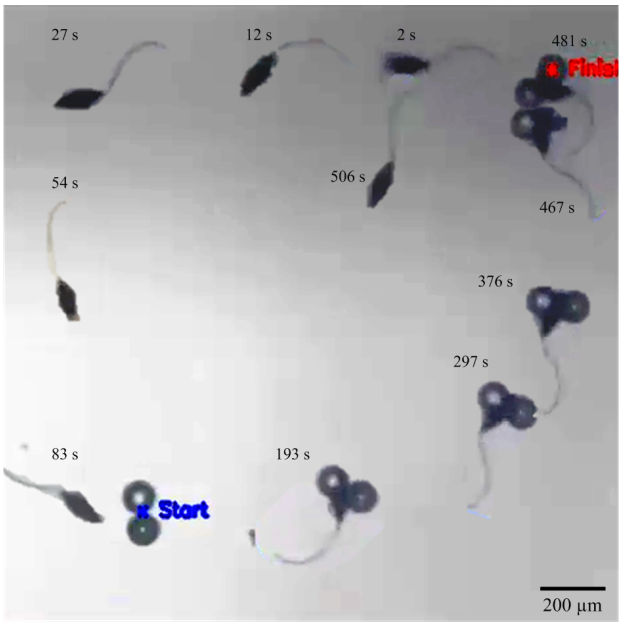

Fig. 1. Manipulation of 2-microbead using a soft microrobotic sperm is achieved in two-dimensional space. At time, $t = 2$ seconds, the microrobot swims toward the 2-microbead at an average speed of 50 μm/s. At time, $t = 96$ seconds, the microrobot comes into contact with the 2-microbead and swims controllably towards the reference position at an average speed of 10.7 μm/s. The microrobotic sperm delivers the microbeads at the reference position at time, $t = 481$ seconds, and breaks free from the microbeads. The blue and red dots represent the initial position of the microbeads and the reference position, respectively. *Please refer to the accompanying video.*

II. Soft Microrobotic Sperm with a Payload

We consider a soft microrobotic sperm with a prolate spheroid head and an ultra thin flexible tail, of length l_{t} and radius r_{t}. The head (with minor diameter $2r_{\mathrm{h}}$) has an average magnetic moment $\mathbf{m}$, lying along its long axis. This magnetic moment enables directional control of the microrobotic sperm under the influence of an external magnetic field $\mathbf{B}$. The microrobotic sperm is contained in a viscous medium with viscosity μ. The directional control of the external magnetic field allows the microrobotic sperm to swim towards microbeads, of diameter D, and achieve

978-1-5386-4841-4/18/$31.00 ©2018 IEEE

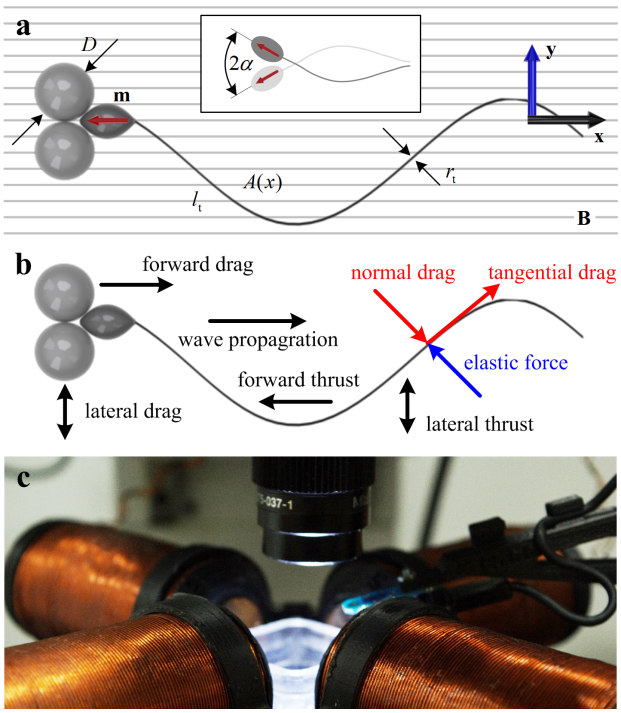

Fig. 2. Microrobotic sperm is used to manipulate microbeads with diameter D. (a) A schematic representation shows a microrobotic sperm in contact with a non-magnetic 2-microbead. The microrobot, with tail length l_t and tail radius r_t, achieves propulsion using its flexible tail under the influence of periodic field $\mathbf{B}$. The prolate spheroid head of the microrobot has magnetization $\mathbf{m}$ that enables directional control along field lines (light gray lines). The inset shows the angle of oscillation (α) of the head. (b) The free-body diagram shows the resultant fluid drag and thrust along the elastic tail. (c) Magnetic fields are generated using 4 coils.

manipulation, as shown in Fig. 2(a). The asymptotic force balance between the drag force acting on the microbeads, pushed along the long axis ($\mathbf{x}$-axis) of the microrobotic sperm, and the net propulsive force [Fig. 2(b)] exerted on the elastic tail is given by [17]

$$-6\pi\mu v_x\left(D+r_h\right)=\int_0^{l_t}\frac{-v_x\alpha-v_y\gamma}{\beta^2\sin\left(kx-\omega t\right)^2+1}\mathrm{d}x, \quad (1)$$

where v_x and v_y are the forward and lateral velocities of the microrobotic sperm, respectively. In (1), $\beta = kA$, where $k = 2\pi/\lambda$ is the wave number and A is the amplitude of a sinusoidal wave of wavelength λ. Further, α and γ are given by

$$\alpha \triangleq C_t+\beta^2 C_n\sin\left(kx-\omega t\right)^2, \quad (2)$$

$$\gamma \triangleq \beta\sin\left(kx-\omega t\right)\left(C_n-C_t\right). \quad (3)$$

In (2) and (3), $\omega = 2\pi f$ is the actuation frequency of the external magnetic field. Further, C_t and C_n are the tangential and normal drag coefficients given by [18]

$$C_t = \frac{8\pi\mu(l_t/r_t)}{3\log(l_t/r_t)}\left(\frac{1+\frac{0.307}{\log(l_t/r_t)}}{1+\frac{0.5}{\log(l_t/r_t)}}\right), \quad (4)$$

$$C_n = \frac{4\pi\mu(l_t/r_t)}{3\log(l_t/r_t)}\left(\frac{1+\frac{0.307}{\log(l_t/r_t)}}{1-\frac{0.5}{\log(l_t/r_t)}}\right). \quad (5)$$

The force balance (1) between the microbead and the microrobotic sperm is valid for the following assumption: The tail is assumed to be moving along $\mathbf{x}$- and $\mathbf{y}$-axis while the magnetic rotation is inducing a pure sinusoidal wave deformation. Under this assumption, the largest theoretical microbead size for manipulation can be determined using (1). In addition, the theoretical limit for the swimming speed for a given microbead size can be predicted in a similar manner.

We solve (1) numerically for a 240-µm-long robotic sperm with tail length and radius of 160 µm and 4 µm, respectively. The minor and major diameters of the prolate spheroid are 40 µm and 80 µm, respectively. The actuation frequency of the external magnetic fields is allowed to vary between 1 Hz to 10 Hz, whereas the diameter of the 2-microbead is increased with a step of 100 µm. The viscosity of the medium is 0.95 Pa.s and the modulus of elasticity of the tail is 0.58 GPa [17]. Fig. 3 shows the influence of the diameter of the 2-microbead on the swimming speed of the robotic sperm. Fig. 3(a) indicates that the speed of the microrobotic sperm decreases with the increased diameter of the payload. The maximum swimming speed of the microrobotic sperm is calculated as 33 µm/s, at $f = 3$ Hz, during collision-free flagellar propulsion. During manipulation of a 2-microbead with diameter of 100 µm, the maximum speed decreases to 24 µm/s, at $f = 2$ Hz. Similarly, the maximum swimming speed decreases to 10.2 µm/s ($f = 2$ Hz) and 4.8 µm/s ($f = 1$ Hz) during manipulation of 2-microbead with diameter of 200 µm and 300 µm, respectively. Fig. 3 shows that the size of the 2-microbead influences the angle of oscillation (α) of the head for all actuation frequencies. Therefore, the speed of the microrobotic sperm decreases with the increased size of the payload owing to the higher drag exerted on the microbeads and head (1) and the decrease in the oscillation angle of the head. Figs. 3(c)-3(f) show the influence of the size of the 2-microbead on the deformation of the flexible tail for a complete cycle.

III. Experimental Results

Micromanipulation experiments are done on the silicon oil-air interface to keep the microbeads and the microrobotic sperm on the same plane. The container is surrounded with 4 electromagnetic coils [Fig. 2(c)]. Each coil (with wire thickness of 0.7 mm and 3200 turns) has length of 80 mm and inner- and outer-diameter of 20 mm and 40 mm, respectively. Microbeads (blue polystyrene particles, Micromod Partikeltechnologie GmbH, Rostock-Warnemuende, Germany) with average diameter of 100 µm are used as payload for the microrobotic sperm. These microrobots are fabricated in a single fabrication step by electrospinning a solution of polystyrene in dimethylformamide [8]. The polystyrene solution contains iron-oxide microparticles with average diameter of 30 µm. Electrospinning of this solution enables the microparticles to be embedded into the polymer matrix of the generated continuous beaded fibers. Finally, soft microrobotic sperms are obtained by cutting the beaded fibers with tail length l_t to achieve a Sperm number of approximately 2.1 [6]. The microrobots are contained with

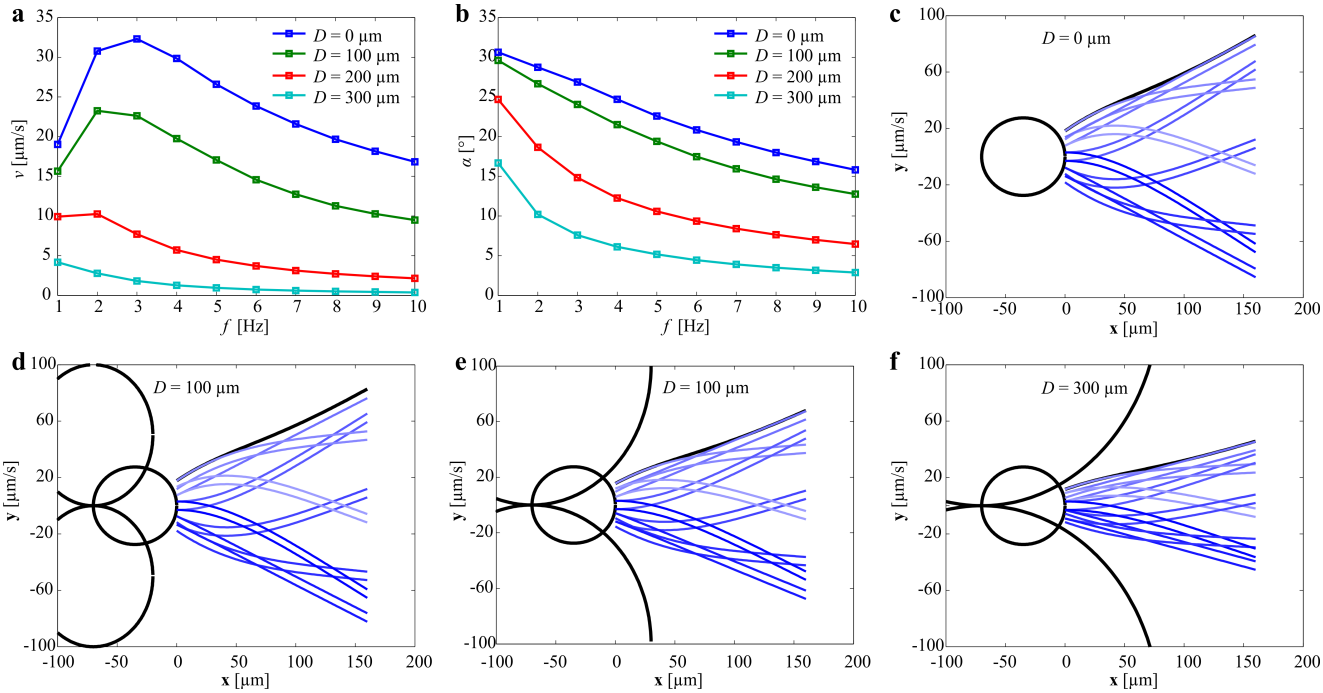

Fig. 3. Simulation results of the microrobotic sperm show the influence of the diameter of the 2-microbead and the actuation frequency on its swimming speed. (a) The speed of the microrobotic sperm is decreased by approximately 21% owing to the total drag exerted on the 2-microbead ($f = 1$ Hz). The speed is decreased by 41% as the diameter of the microbeads is increased with 100 µm in diameter ($f = 1$ Hz). (b) The diameter of the 2-microbead influences the oscillation angle (α) of the head. (c) At $f = 1$ Hz, the speed of the microrobotic sperm is 19 µm/s. (d) At $f = 1$ Hz, the calculated speed of the microrobotic sperm is 16 µm/s during manipulation of 2-microbead with diameter of 100 μm. (e) At $f = 1$ Hz, the calculated speed of the microrobotic sperm is 10 µm/s during manipulation of 2-microbead with diameter of 200 µm. (d) At $f = 1$ Hz, the calculated speed of the microrobotic sperm is 4.5 µm/s during manipulation of 2-microbead with diameter of 300 µm.

the microbeads and controlled by teleoperation with an Exterme 3D pro Joystick (963290-0403, logitech, Newark, USA) that is connected to an NI myRIO board (National Instruments, Austin, Texas, U.S.A). The electromagnetic coils are teleoperated [19] such that uniform field are oriented towards the direction of motion with orthogonal periodic component, at actuation frequency f.

Fig. 4 shows two representative manipulation trials of 2-microbead. In these trials, the reference position (vertical blue line) is provided in any arbitrary location, as shown in Fig. 4(a). The microrobotic sperm is actuated to swim towards the 2-microbead (vertical green line) and inserts its prolate spheroid head between the 2-microbead, as shown in Fig. 1 at $t = 96$ seconds. At this time instant, the speed of the microrobotic sperm is decreased by approximately 75% owing to the increased drag by the 2-microbead [Figs. 4(b) and (c)]. At time $t = 481$ seconds, the microrobotic sperm positions the 2-microbead at the reference position and breaks free. Another representative manipulation trial is shown in Fig. 4(d). The average speed of the microrobotic sperm towards the 2-microbead is 25 µm/s and is decreased to 10 µm/s upon contact with the 2-microbead, as shown in Figs. 4(e) and 4(f). In this trial, the additional drag exerted on the 2-microbead results in a 60% decrease in the speed of the microrobotic sperm. Once the 2-microbead are positioned at the reference position, the actuation frequency is increased to break free from the 2-microbead. The increase in the actuation frequency decreases the amplitude of the elastic deformation owing to the alleviated shear stress. Therefore, the induced flow-field is relatively weak and the microrobotic sperm does not influence the 2-microbead as it swims away. *Please refer to the accompanying video.*

IV. Conclusions and Future Work

Micromanipulation of non-magnetic microbeads is experimentally demonstrated using soft microrobotic sperms driven via controlled oscillating magnetic fields. Our experimental results show that the additional drag caused by a payload of 2-microbead decreases the swimming speed of the microrobotic sperm by approximately 70%, at relatively low actuation frequencies. The average swimming speed of a microrobotic sperm is measured as 0.16 and 0.035 body-length-per-second during collision-free flagellar propulsion and manipulation of non-magnetic 2-microbead with diameter of 100 µm, respectively.

As part of future studies, our soft microrobotic sperms will be used in microassembly of non-magnetic objects. This goal necessitates characterization of the frequency-dependent flow-field that is caused by flagellar propulsion. Our experiments show that the influence of the flow-field on the positioning accuracy of the payload is mitigated at relatively high actuation frequency. Nevertheless, the induced flow-field by the flexible tail after positioning of the microbeads affects the positioning accuracy. Therefore, this flow-field will be further measured using particle velocimetry imaging.

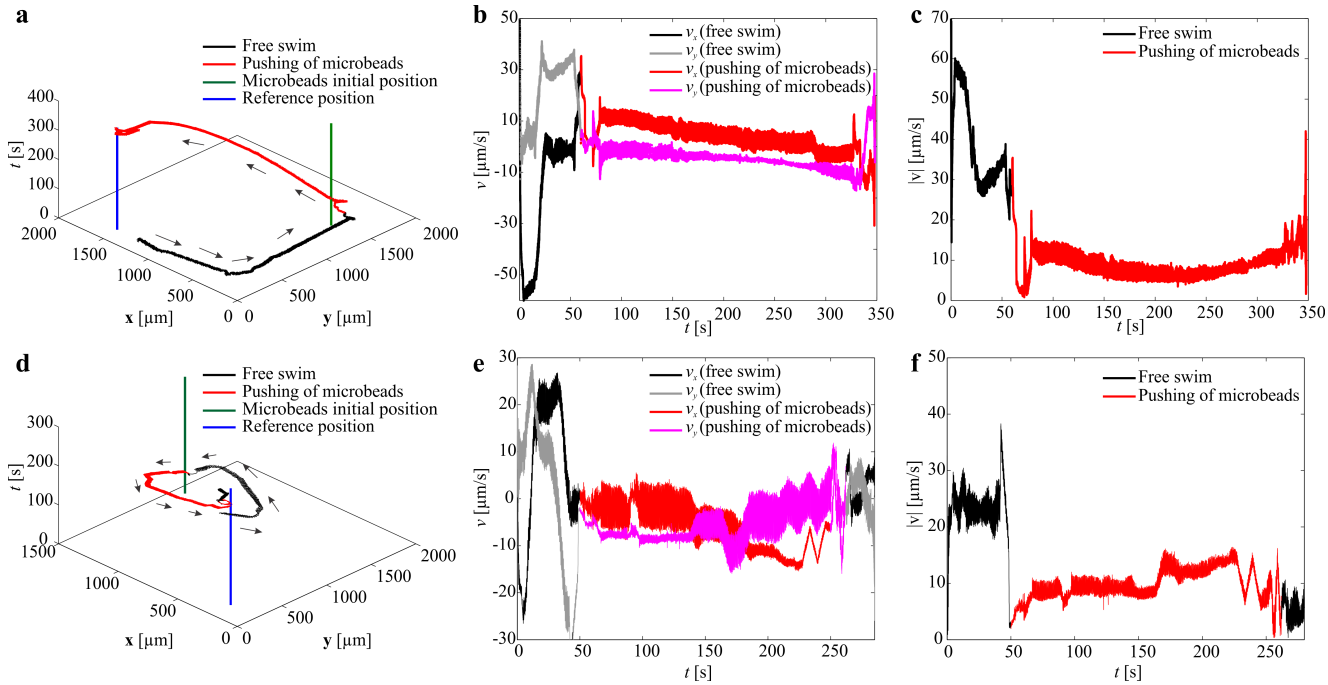

Fig. 4. A representative experimental result of the manipulation of 2-microbead using a soft microrobotic sperm. (a) The black trajectory represents the path taken by the microrobot towards the microbeads before contact. The green vertical line represents the initial position of the 2-microbead. The red trajectory shows the path taken by the microrobot while pushing the 2-microbead toward the reference position (vertical blue line). (b) The speed of the microrobotic sperm decreases once its comes into contact with the 2-microbeads ($t = 60$ seconds). (c) The speed is approximately 45 μm/s before contact with the microbead, and is decreased to approximately 10 μm/s during pushing. (d) Another manipulation trial of 2-microbead is achieved. (e) The velocity components of the microrobotic sperm indicate a decrease in the speed due to the additional drag on the 2-microbeads. (f) The microrobotic sperm swims towards the 2-microbead at an average speed of 24 μm/s and manipulation starts at time, $t = 50$ seconds. At this instant, the speed is decreased to 10 μm/s. At time, $t = 260$ seconds, the microrobotic sperm breaks free from the payload. *Please refer to the accompanying video.*

References

[1] B. J. Nelson, I. K. Kaliakatsos, and J. J. Abbott, "Microrobots for minimally invasive medicine," *Annual Review of Biomedical Engineering*, vol. 12, pp. 55-85, April 2010.

[2] A. Ghosh and P. Fischer, "Controlled propulsion of artificial magnetic nanostructured propellers," *Nano Letters*, vol. 9, pp. 2243-2245, June 2009.

[3] L. Zhang, J. J. Abbott, L. Dong, B. E. Kratochvil, D. Bell, and B. J. Nelson, "Artificial bacterial flagella: fabrication and magnetic control," *Applied Physics Letters*, vol. 94 (064107), February 2009.

[4] K. E. Peyer, L. Zhang, and B. J. Nelson, "Bio-inspired magnetic swimming microrobots for biomedical applications," *Nanoscale*, vol. 5, no. 4, pp. 1259-1272, November 2012.

[5] A. Servant, F. Qiu, M. Mazza, K. Kostarelos, and B. J. Nelson, "Controlled in vivo swimming of a swarm of bacteria-like microrobotic flagella," *Advanced Materials*, vol. 27, no. 19, pp. 2981-2988, April 2015.

[6] E. L. Tony, S. Yu, and A. E. Hosoi, "Experimental investigations of elastic tail propulsion at low Reynolds number," *Physics of Fluids,* vol. 18 (091701), September 2006.

[7] B. Jang, E. Gutman, N. Stucki, B. F. Seitz, P. D. Wendel-García, T. Newton, J. Pokki, O. Ergeneman, S. Pané, Y. Or, B. J. Nelson, "Undulatory locomotion of magnetic multilink nanoswimmers," *Nano Letters*, vol. 15, no. 7, pp. 4829-4833, June 2015.

[8] I. S. M. Khalil, A. F. Tabak, A. Klingner, and M. Sitti, "Magnetic propulsion of robotic sperms at low-Reynolds number," *Applied Physics Letters*, vol. 109 (033701), July 2016.

[9] E. Diller, J. Zhuang, G. Lum, M. Edwards, and M. Sitti, "Continuously distributed magnetization profile for millimeter-scale elastomeric undulatory swimming," *Applied Physics Letters*, vol. 104, April 2014.

[10] I. S. M. Khalil, A. F. Tabak, M. Abou Seif, A. Klingner, B. Adel, and M. Sitti, "Swimming in low Reynolds numbers using planar and helical flagellar waves," in *Proceedings of the IEEE International Conference on Intelligent Robots and Systems (IROS)*, pp. 1907–1912, Vancouver, BC, Canada, September 2017.

[11] J. Zhang and E. Diller, "Millimeter-Scale magnetic swimmers using elastomeric undulations," in *Proceedings of the IEEE/RSJ International Conference of Robotics and Systems (IROS)*, pp. 1706–1711, Hamburg, Germany, September 2015.

[12] D. Ahmed, C. Dillinger, A. Hong, and B. J. Nelson, "Artificial acoustomagnetic soft microswimmers," *Advanced Materials Technologies*, vol. 2, no. 7 (1700050), May 2017.

[13] S. Palagi, A. G. Mark, S. Y. Reigh, K. Melde, T. Qiu, H. Zeng, C. Parmeggiani, D. Martella, A. Sanchez-Castillo, N. Kapernaum, F. Giesselmann, D. S. Wiersma, E. Lauga, P. Fischer, "Structured light enables biomimetic swimming and versatile locomotion of photoresponsive soft microrobots," *Nature Materials*, vol. 15, pp. 647-653, February 2016.

[14] I. S. M. Khalil, A. F. Tabak, K. Sadek, D. Mahdy, N. Hamdi, and M. Sitti, "Rubbing against blood clots using helical robots: modeling and in vitro experimental validation," *IEEE Robotics & Automation Letters*, vol. 2, no. 2, pp. 927-934, April 2017.

[15] S. Martel, C. C. Tremblay, S. Ngakeng, and G. Langlois, "Controlled manipulation and actuation of micro-objects with magnetotactic bacteria," *Applied Physics Letters*, vol. 89, pp. 1-3, December 2006.

[16] J. Gray and G. J. Hancock, "The propulsion of sea-urchin spermatozoa," *Journal of Experimental Biology*, vol. 32, pp. 802814, December 1955.

[17] I. S. M. Khalil, A. F. Tabak, Y. Hamed, M. Elwi, M. Tawakol, A. Klingner, and M. Sitti, "Swimming back and forth using planar flagellar propulsion at low Reynolds numbers," *Advanced Science*, vol. 5, no. 2 (1700461), December 2017.

[18] C. Brennen and H. Winet, "Fluid mechanics of propulsion by cilia and flagella," *Annual Review of Fluid Mechanics*, vol. 9, pp. 339-398, January 1977.

[19] I. S. M. Khalil. K. Youakim, A. Sánchez, and S. Misra, "Magnetic-based motion control of sperm-shaped microrobots using weak oscillating magnetic fields," in *Proceedings of the IEEE International Conference on Intelligent Robots and Systems (IROS)*, pp. 4686–4691, Chicago, USA, November 2014.